Acta Pharmacologica Sinica

www.nature.com/aps

ARTICLE

Investigation of targets and anticancer mechanisms of covalently acting natural products by functional proteomics

Wen-si Zhao[1,2,3], Kai-feng Chen[1,2,3], Man Liu[1], Xing-long Jia[1,4], Yu-qi Huang[1,2], Bing-bing Hao[1], Hao Hu[1], Xiao-yan Shen[4], Qiang Yu[1] and Min-jia Tan[1,2,3,5] ✉

Eriocalyxin B (EB), 17-hydroxy-jolkinolide B (HJB), parthenolide (PN), xanthatin (XT) and andrographolide (AG) are terpenoid natural products with a variety of promising antitumor activities, which commonly bear electrophilic groups (α,β–unsaturated carbonyl groups and/or epoxides) capable of covalently modifying protein cysteine residues. However, their direct targets and underlying molecular mechanisms are still largely unclear, which limits the development of these compounds. In this study, we integrated activity-based protein profiling (ABPP) and quantitative proteomics approach to systematically characterize the covalent targets of these natural products and their involved cellular pathways. We first demonstrated the anti-proliferation activities of these five compounds in triple-negative breast cancer cell MDA-MB-231. Tandem mass tag (TMT)-based quantitative proteomics showed all five compounds commonly affected the ubiquitin mediated proteolysis pathways. ABPP platform identified the preferentially modified targets of EB and PN, two natural products with high anti-proliferation activity. Biochemical experiments showed that PN inhibited the cell proliferation through targeting ubiquitin carboxyl-terminal hydrolase 10 (USP10). Together, this study uncovered the covalently modified targets of these natural products and potential molecular mechanisms of their antitumor activities.

Keywords: natural products; proteomics; ABPP; eriocalyxin B; parthenolide

Acta Pharmacologica Sinica (2023) 44:1701–1711; https://doi.org/10.1038/s41401-023-01072-z

INTRODUCTION

Natural products bearing great structural diversity exhibit therapeutic activities for various diseases, such as bacterial and fungal infections, inflammation, neurodegenerative diseases, diabetes and cancer [1–3]. Approximately 25%–50% of marketed drugs are derived from natural products [4]. A subset of natural products bearing electrophilic moieties are capable of formation of irreversible bonds with nucleophiles of proteins. These covalent inhibitors were considered to have advantages of improved potency, selectivity, and duration of the pharmacodynamics effects [5], suggesting covalent inhibitors from natural sources provide a rich resource for drug discovery and development.

Natural products eriocalyxin B (EB), 17-hydroxy-jolkinolide B (HJB), parthenolide (PN), xanthatin (XT) and andrographolide (AG) are all terpenoid active ingredients extracted from traditional medicinal or folk medicine. EB was used as an anti-inflammatory remedy in traditional Chinese medicine and showed potent anti-inflammatory effects [6, 7]. HJB was extracted from Chinese medicinal herb Lang-du, which was used for the treatment of indigestion and edema in folk medicine [8]. PN was the bioactive ingredient of the plant feverfew, which was used for the alleviation of fever, rheumatoid arthritis, migraine, toothache, stomachache [9, 10]. XT was isolated from the plant *Xanthium L.*, which could treat diseases such as arthritis and nasal sinusitis [11, 12]. AG was the major active component of a medicinal plant *A. paniculata* and exerted beneficial effects on inflammation [13–15]. Despite of varied structural skeletons, they commonly bear electrophilic groups (α,β–unsaturated carbonyl groups in all of them, and epoxides in HJB and PN) (Fig. 1a), which are capable of covalently modifying protein cysteine residues and potentially regulate the functions for a plethora of proteins [16]. Recently, these compounds have been reported to have a variety of antitumor activities. They share some similarly impacted pathways, but they also have distinct pharmacological effects. EB induced apoptosis of leukemia cells by suppressing NF-κB activity and dysregulation of MAPK-signaling pathway [17]. HJB inhibited JAK/STAT3 pathway by targeting the JAK family kinases and inhibited PI3K-Akt pathway to induce apoptosis of cancer cells [18, 19]. PN impaired cancer pathogenicity through regulating multiple cellular signaling pathways, such as IKK-β and NF-κB signaling [20, 21], JAK/STAT3 signaling [22] and FAK1 signaling [23]. XT activated endoplasmic reticulum stress to induce apoptosis in hepatoma cells [24], targeted JAK2 and IKKβ to preferentially inhibit the growth of cancer cells with constitutively activated STAT3 and p65 [11] and inhibited mTOR signaling to suppress colon cancer progression [25]. AG inhibited ER-α receptor, PI3K/AKT/mTOR signaling, THO complex and suppressed cell proliferation, induced cell cycle arrest and apoptosis of various cancer cells [13, 26, 27]. However, the direct covalent targets and

[1]State Key Laboratory of Drug Research, Shanghai Institute of Materia Medica, Chinese Academy of Sciences, Shanghai 201203, China; [2]University of Chinese Academy of Sciences, Beijing 101408, China; [3]Zhongshan Institute for Drug Discovery, Shanghai Institute of Materia Medica, Chinese Academy of Sciences, Zhongshan 528400, China; [4]Department of Pharmacology, School of Pharmacy, Fudan University, Shanghai 201203, China and [5]Jiangsu Key Laboratory of Marine Pharmaceutical Compound Screening, College of Pharmacy, Jiangsu Ocean University, Lianyungang 222005, China
Correspondence: Min-jia Tan (mjtan@simm.ac.cn)
These authors contributed equally: Wen-si Zhao, Kai-feng Chen

Received: 31 October 2022 Accepted: 23 February 2023
Published online: 17 March 2023

molecular mechanisms of action are still largely unclear, which greatly limits the development of these compounds.

Due to the high throughput and increasing sensitivity, mass spectrometry (MS)-based proteomics provides the most accessible opportunity to reveal the signaling pathway alterations and identify the potential targets [28, 29], and has become one of the most effective ways to address above-mentioned issues. Quantitative proteomics takes advantage of unbiased analysis for global protein expression changes and signaling pathway alterations [28, 30, 31]. Activity-based protein profiling (ABPP), which integrates reactive probes, affinity purification and proteomics technology, has facilitated the system-wide discovery of potential targets and binding sites of covalent inhibitors [32–37]. One of the most widely used platform to analyze cysteine reactivity to covalent inhibitors is isoTOP (isotopic tandem orthogonal proteolysis)-ABPP developed by Cravatt et al. [32]. However, the isotopic labels were introduced by in vitro click chemistry, thus quantification accuracy was impaired by operational variations [34, 38–40]. Other strategies such as multiplexed thiol reactivity profiling (MTRP) developed by Yang et al. utilized iTRAQ based high-throughput quantification, but suffered from the ratio compression effect [41–44]. Herein, we integrated stable-isotope labeling by amino acids in cell culture (SILAC) and cleavable azide-biotin tags into ABPP workflow [40, 45]. This approach can take advantage of accurate quantification and minimize potential operational variation of SILAC to quantify the reactivity of each labeled residue, providing an easy, sensitive, universal and relatively low-cost approach to systematically identify the covalent binding sites of structurally diverse natural products.

In this study, we integrated quantitative proteomics approach and this ABPP platform to system-wide identify involved pathways of EB, HJB, PN, XT, AG, and the preferentially modified targets of EB and PN. Quantitative proteomics results showed all these compounds affected the ubiquitin mediated proteolysis pathways. ABPP platform identified diverse potential covalent binding proteins of EB and PN. Bioinformatics analysis suggested that those potential binding proteins were also involved in the protein polyubiquitination pathway. Further target validation and activity evaluation also showed that PN inhibited the proliferation of MDA-MB-231 cells through targeting ubiquitin carboxyl-terminal hydrolase 10 (USP10). This study uncovered the potential targets and molecular mechanisms of covalent inhibitors from natural sources, and provided a rich resource for drug discovery and development for triple-negative breast cancer.

MATERIALS AND METHODS

Reagents

The XT was isolated from the aerial parts of *Xanthium mogolium Kitag*, as described previously [46]. The HJB was isolated from *Euphorbia fischeriana*, as described previously [47]. EB (Shanghai YuanYe Biotechnology Co., Ltd., Shanghai, China), PN (Sigma-Aldrich, St. Louis, MO, USA) and AG (Sigma-Aldrich, St. Louis, MO, USA) were dissolved in DMSO and each stock solution was stored in −20 °C. Trypsin was purchased from Hualishi Scientific (Beijing, China). [$^{12}C_6$, $^{14}N_4$]-arginine (R0), [$^{12}C_6$]-lysine (K0), [$^{13}C_6$, $^{15}N_4$]-arginine (R10) and [$^{13}C_6$]-lysine (K6) were from Silantes (Munich, Germany). C18 Zip Tip was from Millipore Corporation (Billerica, MA, USA). DUB activity assay kit was purchased from Cayman Chemical (Ann Arbor, MI, USA) and USP10 was purchased from Boston Biochem (Cambridge, MA, USA). Other chemicals were purchased from Sigma-Aldrich unless noted otherwise.

Cell culture

The MDA-MB-231 cells were grown in 1640 medium (Hyclone, South Logan, UT, USA) supplemented with 10% of FBS, 100 U/mL penicillin, 0.1 mg/mL streptomycin, 2.05 mM *L*-glutamine, and 25 mM HEPES. For identification of EB/PN targets, the MDA-MB-231 cells were cultured in SILAC media. MDA-MB-231 cells treated with DMSO were cultured in heavy SILAC 1640 media (supplemented with K6 and R10), whereas MDA-MB-231 cells treated with EB/PN were cultured in light 1640 media (supplemented with K0 and R0). Cells were grown for at least 6 times of passages until the SILAC labeling efficiency met the requirement (>95%).

Cell viability assays

About 2500–3500 cells were seeded in 96-well plates with 100 μL of medium for 24 h and then treated with different concentrations of compounds for 72 h. CCK-8 (Dojindo Molecular Technologies Inc., Kumamoto, Japan) was used to measure cell viability as described previously [48].

ABPP analysis of potential targets

After MDA-MB-231 cells were grown to 90%–100% confluency, the medium was removed and replaced with fresh medium with or without 100 μM EB/PN. Then the cells were incubated at 37 °C for 1 h and harvested to prepare EB/PN-treated and control proteomes, respectively. Samples were prepared in five biological replicates. Cells were collected and sonicated in PBS. BCA protein assay kit (Beyotime Biotechnology, Shanghai, China) was used to determine the protein concentration. Then isotopically heavy (DMSO) or light (EB/PN) proteomes were mixed in a 1:1 ratio. The protein lysates were reacted with iodoacetamide-alkyne (IA, 100 μM) for 1.5 h in darkness at room temperature. Two hundred micromole Diazo Biotin-Azide (Jena Bioscience, Jena, Germany) were appended to probe-labeled proteins with 5 mM ascorbic acid, 800 μM THPTA and 100 μM $CuSO_4$. The click chemistry was allowed to react for 3 h. After the click chemistry step, the mixed samples were precipitated with chilled (−20 °C) acetone. The precipitate was washed with acetone for 7 times, and the supernatant was discarded after centrifugation. The pellet was suspended in PBS (adjust pH = 8) and was digested by trypsin, an enzyme to-substrate ratio of 1:50 (*w*/*w*) at 37 °C for 4 h. Next, the samples were reduced by 5 mM dithiothreitol (DTT) at 56 °C for half an hour, and reacted with 15 mM iodoacetamide (IAA) in darkness at room temperature for half an hour. Unreacted iodoacetamide was quenched by 30 mM cysteine at 25 °C for another 1 h. The samples were digested by trypsin, an enzyme to substrate ratio of 1:100 (*w*/*w*) at 37 °C for another 4 h. The peptide solutions were diluted with SDS to a final concentration of 0.1% and incubated with 100 μL of streptavidin-agarose beads (Pierce, Rockford, IL, USA) for 30 min at room temperature [49]. The beads were washed with 0.1% SDS twice and PBS for 7 times. The beads were incubated with 100 μL sodium dithionite (100 mM) for 30 min twice and washed with H_2O (3 × 100 μL) [40, 45], for which all the supernatant was then pooled and desalted with OMIX C18 cartridges (Agilent, Palo Alto, CA, USA).

Proteome preparation for protein profiling

In order to balance the depth of proteome coverage and compound efficacy/toxicity, we treated MDA-MB-231 cells with each natural product at the concentration of tenfold of IC_{50} for 16 h. Cells were harvested by centrifugation at 1000 × *g* for 5 min. The pellet was washed with ice-cold PBS buffer for three times and then resuspended in lysis buffer (8.0 M Urea in 100 mM NH_4HCO_3 supplemented with 2× protease inhibitor cocktail) on ice for half an hour. The cells were sonicated for 2 min (2 s sonication with 5 s intervals, 30% power). After centrifugation at 21,130 × *g* at 4 °C for 20 min, the precipitates were discarded. BCA protein assay kit (Beyotime Biotechnology, Shanghai, China) was used to determine the protein concentration. The samples were reduced by 5 mM DTT at 56 °C for half an hour, followed by incubation with 15 mM IAA in darkness at room temperature for half an hour. The excess IAA was quenched by 30 mM cysteine at 25 °C for another 30 min. The protein solution was diluted with 100 mM NH_4HCO_3 (pH 8.0) and then was digested by trypsin for two times, an enzyme to-substrate ratio of 1:50 (*w*/*w*) at 37 °C for 16 h and an enzyme to-substrate ratio

of 1:100 (*w/w*) at 37 °C for 4 h. Sep-Pak C18 cartridges (Waters, Milford, MA, USA) was used for peptide desalting.

Tandem mass tag (TMT) labeling and HPLC fractionation
TMT labeling was carried out with TMT Mass Tagging Kits (Thermo Fisher Scientific, San Jose, CA, USA) [50]. The labeling efficiency of TMT was checked with an EASY-nLC 1000 system coupled to an Orbitrap Fusion mass spectrometer (Thermo Fisher Scientific, San Jose, CA, USA). After checking the labeling efficiency, TMT tagged peptides from each sample were pooled together and desalted by Sep-Pak C18 cartridges. Then samples were subjected to high pH reverse phase HPLC using a Waters XBridge Prep C18 column (5 μm particles, 4.6 mm × 250 mm) to separate the tryptic peptides. The mobile phase A solvent (pH = 10) contained ammonium hydroxide solution and 2% acetonitrile, and the mobile phase B consisted of 2% mobile phase A and 98% acetonitrile. The mobile phase flow rate was 1 mL/min. The linear gradient for separation was 0% to 5% B in 2 min, from 5% to 12% B in 8 min, to 33% B in 57 min, to 95% B in 2 min. The peptides were combined into 20 fractions and vacuum-dried for further experiments.

Mass spectrometry analysis
For protein profiling, the sample was dissolved in buffer A (0.1% formic acid, 2% acetonitrile) and loaded onto 20 cm C18 reversed phase capillary analytical column (ReproSil-Pur 120 C18-AQ, 1.9 μm particle size, 120 Å pore size, Dr. Maisch GmbH, Germany) via the autosampler connected to an EASY-nLC 1200 HPLC system (Thermo Fisher Scientific, Waltham, MA, USA). The peptides were eluted with a linear gradient of buffer B (0.1% formic acid, 90% acetonitrile) from 6% to 30% in 57 min, followed by an increase to 45% in 4 min, then a steep increase to 80% in 4 min at a constant flow rate of 300 nL/min. Then the eluted peptides were ionized and sprayed into a Q Exactive HF-X mass spectrometer (Thermo Fisher Scientific, Waltham, MA, USA). The mass spectrometric analysis was performed in a positive mode. The peptides with a range of *m/z* 350–1550 were analyzed by Orbitrap mass analyzer with a resolution of 60,000 at *m/z* 200. The automatic gain control (AGC) target was set to 3×10^6 and maximum ion injection time (IT) to 45 ms. The 20 most intense ions were isolated and subjected to fragmentation via higher-energy collisional dissociation (HCD) with a normalized collision energy (NCE) of 32%. Then, the ion fragments were analyzed in the Orbitrap at a resolution of 15,000 at *m/z* 200. The isolation window was 0.8 m/z. The dynamic exclusion duration was set to 30 s, and the charge exclusion was set as 1+ and ≥6+.

For target identification, the sample was loaded onto 20 cm C18 reversed phase capillary analytical column (3 μm particle size, 90 Å pore size, Dikma Technologies, Lake Forest, CA, USA) via the autosampler connected to an EASY-nLC 1000 HPLC system (Thermo Fisher Scientific, Waltham, MA, USA). The peptides were eluted with a linear gradient of buffer B (0.1% formic acid, 90% acetonitrile) from 5% to 7% in 13 min, from 7% to 10% in 20 min, followed by an increase to 25% in 55 min, from 25% to 45% in 22 min, then a steep increase to 80% in 3 min at a constant flow rate of 300 nL/min. Then the eluted peptides were ionized and sprayed into a Orbitrap Fusion mass spectrometer (Thermo Fisher Scientific, San Jose, CA, USA). The mass spectrometric analysis was performed in a positive mode. The peptides with a range of *m/z* 300–1400 were analyzed by Orbitrap mass analyzer with a resolution of 120,000 at *m/z* 200. The automatic gain control (AGC) target was set to 5×10^5 and maximum ion injection time (IT) to 50 ms. MS/MS acquisition was performed in top speed mode with 3 s cycle time. The most intense ions were isolated and subjected to fragmentation via HCD with a normalized collision energy (NCE) of 32%. The ion fragments were analyzed in the ion trap. The isolation window was 1 *m/z*. The dynamic exclusion duration was set to 50 s. Ions with a single charge or more than six charges were excluded from tandem mass fragmentation.

Data analysis
The raw data was analyzed by MaxQuant (v1.5.3.8) [51] and the built-in Andromeda search engine against a Uniprot human sequence database (updated on 8/24/2018, 95128 sequences), enabling potential contaminants and the reversed versions of all sequences. Trypsin/P was chosen as the digestion enzyme and up to 2 missed cleavage were allowed. The false discovery rate (FDR) cut off for both peptides and proteins is 0.01. The rest of the main parameters are as follows. For protein profiling, TMT (N-terminus and K) and carbamidomethylation (C) were set as fixed modifications, oxidation (M) and acetylation (Protein N-terminal) were set as variable modifications. For Target identification, carbamidomethylation (C), ABPP (C), oxidation (M) and acetylation (Protein N-terminal) were all set as variable modifications. For target identification, the R ratio was calculated with the MS1 chromatographic peak ratios for heavy (DMSO-treated) over light (EB/PN-treated) samples. The R ratios of biological replicates were averaged, and the mean value was reported as its final R ratio. Cases were excluded from further analysis when large variability in R ratios across multiple replicate runs were observed (standard deviation >2/3 of the mean) or when R ratios were not quantified in three or more replicate runs [34]. Those probe-modified sites that only occurred in heavy samples with good reproducibility (three or more replicates were quantified across five replicates) were retained for further analysis.

LC–MS/MS analysis of USP10
Purified USP10 at a final concentration of 100 nM were incubated with parthenolide (10 μM) at room temperature for 30 min. Then the USP10 proteins were separated by SDS-PAGE. The gel slices were cut off from the PAGE and digested in gel [52]. The compound-modified peptide spectra were manually inspected using stringent criteria as previously described [52].

Expression of USP10C40A mutant and gel-based ABPP
293T cells were plated in 6-well flat-bottom plates at 1,000,000 cells/well. Cells were infected with lentiviral particles delivering either pLVX-USP10-Flag WT control or C40A mutant plasmid. After infection puromycin was added to select positive clone. The expression of USP10 was validated through Western blot. USP10 WT and C40A mutant proteins were enriched through immunoprecipitation with anti-Flag M2 affinity gel (Sigma-Aldrich, St. Louis, MO, USA). Enriched USP10 WT and C40A mutant proteins were preincubated with DMSO or PN (50 μM) at room temperature for 30 min. Samples were then incubated with 5-IAF (1 μM) at 37 °C in darkness for another 30 min. Proteins were separated by SDS-PAGE. Labeled proteins were visualized by Typhoon FLA 9500 scanner and silver staining was used as the loading control.

USP10 knockdown
Briefly, MDA-MB-231 cells were plated in 12-well flat-bottomed plates at 400,000 cells/well. Cells were infected with lentiviral particles, at a multiplicity of infection = 100, delivering USP10 or negative control shRNA (Genomeditech Co. Ltd, Shanghai, China). Medium were changed on day 3. Puromycin (Selleck Chemicals, Houston, TX, USA) was added to reach a final concentration of 0.5 μg/mL on day 5, and cells were cultured in the presence of puromycin for a week prior to experimental use. USP10 expression was quantified by qRT-PCR and Western blot for validation.

The measurement of deubiquitinating enzyme activity in vitro
Purified USP10 (20 nM) were preincubated with different concentrations of PN in DUB assay buffer (without DTT) at 25 °C for 1 h. After incubation, deubiquitinating enzyme activity in vitro was measured using DUB activity assay kit according to the manufacturer's instruction (Cayman Chemical, Ann Arbor, MI, USA).

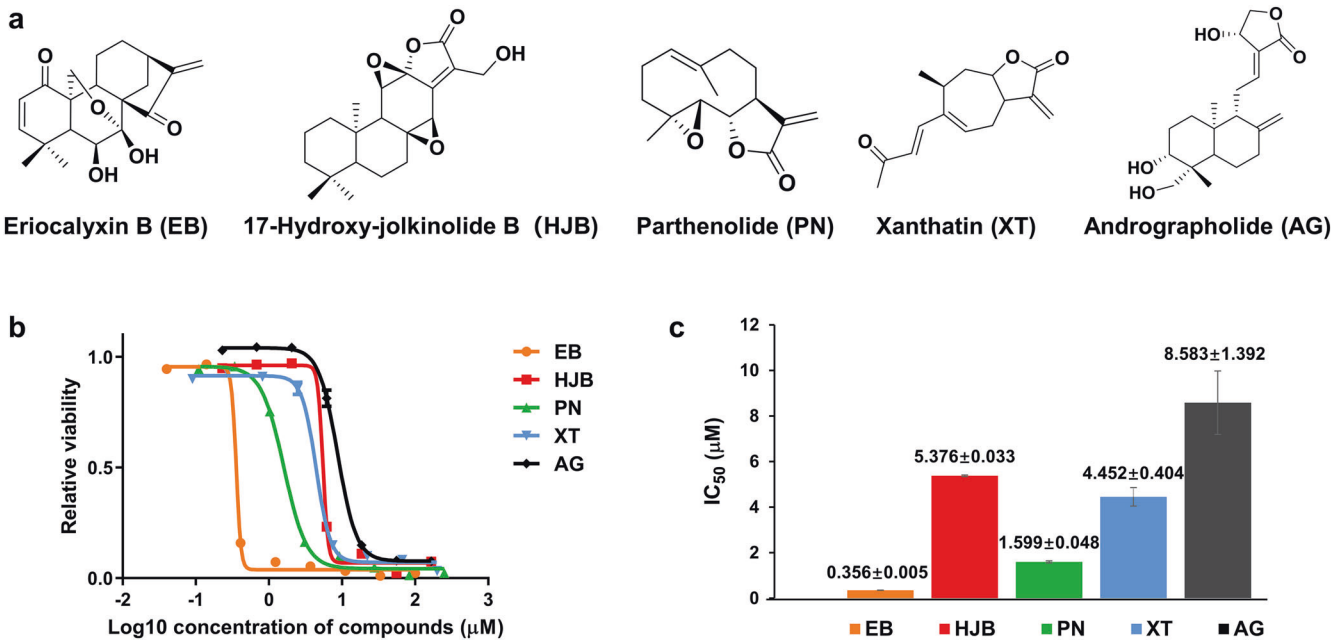

Fig. 1 EB, HJB, PN, XT, AG inhibited breast cancer cell proliferation. **a** Structure of EB, HJB, PN, XT and AG. **b** Dose-dependent effects on MDA-MB-231 cells evaluated at 72 h of treatment in three biological replicates. Data were presented as mean ± SEM. **c** IC_{50} value of five natural products. Data were presented as mean ± SD.

Western blot

Cells were washed twice with cold PBS, and then boiled with loading buffer at 99 °C for 5 min. The protein samples were separated by 12% sodium dodecyl sulfate polyacrylamide gel electrophoresis (SDS-PAGE), and further transferred to NC membrane. Then the membrane was blocked with 5% BSA dissolved in PBST (1× PBS and 0.1% Tween 20) for 2 h at room temperature. After incubated with primary antibody for overnight at 4 °C, the membrane was washed six times with PBST. Sequentially the membrane was incubated with second antibody for 45 min at room temperature. Then the membrane was washed six times with PBST again. Finally, the membrane was detected by the ImageQuant LAS 4000 system (GE Healthcare, Little Chalfont, Buckinghamshire, UK).

Network analysis

Cytoscape (version 3.7.1) software based on the STRING database (version 11.0) was used to analyze protein−protein interactions of the differentially expressed proteins [53, 54]. Interactions with active interaction sources from experiments and databases and an interaction score ≥0.7, were exported from STRING for Cytoscape analysis. Molecular Complex Detection (MCODE), a plugin of Cytoscape, was further applied to analyze highly connected regions [55]. Cluster score cutoff is 10.

Enrichment analysis for differentially expressed proteins

Proteins meeting criteria were subjected to WebGestalt (http://www.webgestalt.org/) for more comprehensive, powerful, flexible and interactive functional enrichment analysis [56]. Gene Ontology (GO) database and Kyoto Encyclopedia of Genes and Genomes (KEGG) database were utilized to assist on exploration of the molecular mechanisms. The adjusted *P* value (Benjamini−Hochberg correction) cutoff is 0.05.

RESULTS

EB, HJB, PN, XT, and AG impair breast cancer cell proliferation

Cell counting kit-8 (CCK-8) assay was used to measure the anticancer effects of EB, HJB, PN, XT, and AG on triple-negative breast cancer cell line MDA-MB-231. The cells were treated with these compounds in a dosage-dependent manner for 72 h, with DMSO as control. As shown in Fig. 1b, all five natural products showed dose-dependent growth inhibition on MDA-MB-231 cells with a half inhibitory concentrations (IC_{50}) ranging from 0.3 to 10 μM. Among them, EB and PN showed relatively higher inhibitory activity with the IC_{50} as 0.356 μM and 1.599 μM, respectively (Fig. 1c). This result suggested the potential antitumor activities of the five natural products at cellular level.

Characterization of global protein expression for the five natural products

To understand and compare the molecular mechanisms among these five natural products, we performed tandem mass tag (TMT)-based quantitative proteomics survey. MDA-MB-231 cells were treated with each natural product at the concentration of tenfold of IC_{50} for 16 h. Cell lysates were extracted, and the proteins were quantified by LC-MS/MS analysis following trypsin digestion and TMT labeling (Fig. 2a). A total of 10,111 proteins were identified, in which 8604 proteins were quantified in at least two biological replicates. Correlation analysis was performed to evaluate the data quality. Correlation coefficients for all five compounds were above 0.9 (Supplementary Fig. S1), suggesting good reproducibility among biological replicates. In the EB, HJB, PN, XT, AG-treated cells, 799, 717, 699, 1337, and 921 proteins showed significant expression difference between the treatment and control groups (*P* value < 0.05 and fold change >1.2) [57, 58], respectively (as shown in Supplementary Tables S1–S5).

GO Biological Process enrichment analysis showed all these compounds affected proteasomal protein catabolic process, RNA catabolic process, regulation of cell cycle phase transition and chromosome segregation (Fig. 2b). KEGG pathway enrichment analysis showed that all these compounds impacted the ubiquitin-mediated proteolysis pathways (Fig. 2c), which suggested that these five natural products might affect cell viability via regulation of protein ubiquitination. The expression levels of proteins involved in "Protein polyubiquitination" and "Proteasomal protein catabolic process" pathways were compared: many proteasome subunits like PSMD1, PSMB7, PSME1 were commonly downregulated and some E3 ubiquitin-protein ligase like RNF34, FBXO11, MYLIP were

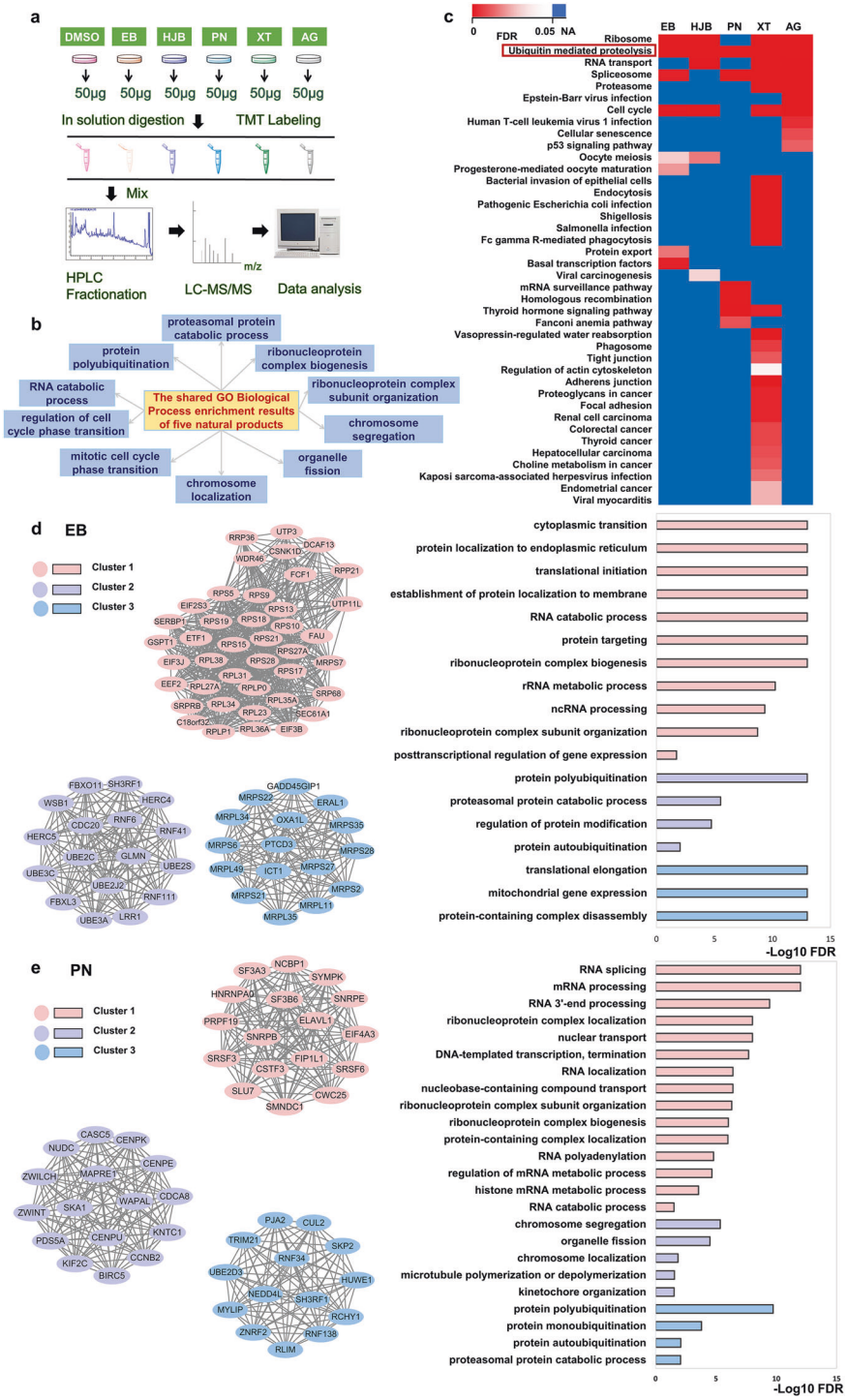

Fig. 2 Characterization of global protein expression for five natural products. (a) The workflow of the TMT-based quantitative proteomic profiling of MDA-MB-231 cells with treatment of DMSO, EB, HJB, PN, XT and AG. **(b)** The shared GO Biological Process enrichment results of five natural products. **(c)** KEGG pathway enrichment analysis of significantly differentiated proteins (P value < 0.05, fold change > 1.2) of five natural products. The global heatmap showing the enriched pathways with each natural products compared to DMSO treated in MDA-MB-231 cells. The color is according to FDR value, and the darkest blue represents N/A. (**d** and **e**) Protein-protein interaction network of significantly differentially expressed proteins of EB and PN, respectively. The top 3 clusters of highly interconnected networks were exhibited. Interaction networks of EB/PN-regulated proteins were listed in gene names, based on STRING database. Cluster 1 of EB: MCODE score = 30.5, nodes = 41, edges = 610. Cluster 2 of EB: MCODE score = 17, nodes = 17, edges = 136. Cluster 3 of EB: MCODE score = 16, nodes = 16, edges = 120. Cluster 1 of PN: MCODE score = 17, nodes = 17, edges = 136. Cluster 2 of PN: MCODE score = 16, nodes = 16, edges = 120. Cluster 3 of PN: MCODE score = 14, nodes = 14, edges = 91. GO Biological Process enrichment analysis was performed in each cluster.

upregulated (Supplementary Fig. S2). Notably, the expression levels of CDC20 and CUL2 proteins were significantly affected in four out of the five natural product-treated samples. CDC20 is a key cofactor of the anaphase-promoting complex or cyclosome (APC/C) E3 ubiquitin ligase with a therapeutic potential for the treatment of cancers [59, 60]. Notably, each natural product also showed uniquely affected pathways. For examples, EB impacted the pathways of protein export (FDR = 0.025301) and basal transcription factors (FDR = 0.005756); PN was associated with pathways of mRNA surveillance pathway (FDR = 0.000122) and homologous recombination (FDR = 3.45E-08); XT affected the pathways related to phagosome (FDR = 0.012649), focal adhesion (FDR = 0.00706), and regulation of actin cytoskeleton (FDR = 0.047802); AG was related with cellular senescence (FDR = 0.016632) and p53 signaling pathways (FDR = 0.021135). The differences of the enriched pathways implied that the five natural products could also impair cell viability via distinct mechanisms. This proteomics data provide rich information on the pathways perturbed by these natural products, which is of benefit to dissect the molecular mechanisms underlying their antitumor activity.

We further subjected the significantly differentially expressed proteins to protein−protein interaction analysis using Cytoscape software and the STRING database. MCODE was further applied to construct highly connected networks and subsequently subjected to gene ontology-biological process analysis by WebGestalt (Supplementary Figs. S3–S5). For EB-regulated proteins, the most highly enriched cluster contained 41 proteins with 610 edges, which were associated with protein localization to endoplasmic reticulum, establishment of protein localization to membrane, protein targeting, translational initiation and RNA catabolic process (Fig. 2d). Ubiquitination-related proteins constituted the second highest enriched cluster (17 proteins with 136 edges), suggesting that EB could actively participate in the ubiquitination-mediated regulation of protein function. In PN-treated cells, the most enriched cluster consisted of 17 proteins with 136 edges, relating with RNA splicing, mRNA processing and RNA 3′-end processing (Fig. 2e). The next two clusters were involved in cellular component organization and localization (the second cluster) and protein ubiquitination (the third cluster). Previous studies reported that PN directly interacted with ubiquitin-specific peptidase 7 (USP7), and promoted the ubiquitination and degradation of β-catenin in Wnt signaling pathways [61]. Moreover, PN induced ubiquitination of MDM2 and resulted in the activation of p53 and other MDM2-regulated tumor-suppressor proteins [62]. These studies were consistent with our bioinformatics analysis.

ABPP to map EB and PN targets in MDA-MB-231 cells

Due to the higher proliferation inhibitory activity of EB and PN, we developed an ABPP platform to identify their preferentially modified targets and their covalently modified amino residues. ABPP was performed in a competitive manner, in which EB/PN competed with the cysteine-reactive iodoacetamide-alkyne (IA) against covalent targets. MDA-MB-231 cells cultured in heavy or light medium were treated with DMSO or EB/PN respectively. Then, the extracted proteins were mixed at 1:1 ratio and labeled with IA. After click reaction with biotin-azo-azide, tryptic digestion, affinity enrichment, and reductive cleavage of azo-bond, probe-modified peptides were analyzed by LC-MS/MS. Thus, the exact residue modified by IA could be determined and the heavy (DMSO-treated group) to light (EB/PN-treated group) ratios for probe-modified peptides could be quantified. The enrichment efficiencies were all above 98%, indicating performance of our ABPP platform was similar with published data [63]. Since the peptides covalently bound by EB/PN were no longer available for IA-labeling, the peptides targeted by EB/PN are expected to be of high heavy-to-light ratios (Fig. 3a).

The distributions of competitive ABPP ratios (R values) were presented in Fig. 3b. Those probe-modified sites, with R value greater than 5 or only being identified in heavy samples for more than or equal to three times out of five replicates, were considered as potential covalent binding sites of the natural products [34, 64]. By this standard, we obtained 65 and 643 potential covalent binding sites on 60 and 519 proteins for EB and PN, respectively (Supplementary Tables S6, S7). As shown in Supplementary Fig. S6a, the abundance of these potential target proteins rarely distributed in the areas of high protein abundance, which suggested the interaction between compounds and potential targets had no obvious bias against protein cellular abundance. We then calculated the percentage of potential covalent targets that could be found in DrugBank (Fig. 3c). After integrating the potential targets of EB and PN, we found 28 (5%) of the potential targets indexed in DrugBank proteins, and 72% of these 28 potential targets possessed enzymatic activities by functional classification analysis. Notably, 95% (554) of the potential targets did not match to DrugBank database, and these proteins belonged to diverse functional classifications, including enzymes, transcriptional factors, transporters and receptors. According to a database containing 628 unique priority targets that were crucial to cell viability or growth by genome-scale CRISPR–Cas9 screens [65], we evaluated the tractability of the potential targets of EB and PN. In the database, the 628 priority targets were categorized into three groups according to their tractability evidences with group 1 as the highest and group 3 as the lowest. Among the potential targets of EB, kinetochore-associated protein 1 (KNTC1) and mannose-1-phosphate guanyltransferase beta (GMPPB) were assigned to tractability group 2, and condensin complex subunit 1 (NCAPD2), dynactin subunit 6 (DCTN6), ubiquitin-conjugating enzyme E2 S (UBE2S) and zinc phosphodiesterase ELAC protein 2 (ELAC2) were assigned to tractability 3. Among the potential targets of PN, DNA methyltransferase 1 (DNMT1), epidermal growth factor receptor (EGFR) and fatty acid synthase (FASN) were assigned to tractability group 1, and there were 22 potential targets classified into tractability group 2 and 22 potential targets into group 3 (Fig. 3d). Notably, DNMT1, EGFR, and FASN in tractability group 1 are all FDA-approved drug targets and play important roles in cancer initiation and progression [66–68]. The above results offered insights into priority of subsequent target validation.

GO Biological Process enrichment analysis showed the potential covalent targets for EB and PN were both associated with protein polyubiquitination, RNA splicing and mRNA processing (Fig. 3e). EB impacted the biological processes of dicarboxylic acid metabolic process, cellular modified amino acid biosynthetic and metabolic process, one-carbon metabolic process and coenzyme metabolic process. PN was related with proteasomal protein catabolic process, regulation of mRNA metabolic process, nuclear transport, ribonucleoprotein complex biogenesis, localization and subunit organization. Since quantitative proteomics analysis implied that EB and PN might share similar molecular mechanisms (i.e., regulation of protein ubiquitination), we compared the potential targets and potential covalently modified sites between EB and PN to discover their commonly shared potential targets. The Venn diagram showed EB and PN shared 4 potential binding sites and 11 potential targets (Fig. 3f). However, these targets were not reported to be associated with protein ubiquitination regulation, which suggested EB and PN might interact with different targets in ubiquitination-regulated pathways.

Biochemical validation of USP10 as a target of PN

Since both quantitative proteomics and ABPP experiment implied that PN had an impact on protein ubiquitination regulation (FDR = 3.39592E-07 in proteomics enrichment result, FDR = 7.04351 E-09 in ABPP enrichment result) and previous researches reported some ubiquitination related proteins like USP7, USP47 as targets of PN [61, 69], we sought to investigate how PN affected this biological process in MDA-MB-231 cell line. Western blotting analysis revealed that ubiquitin signals were significantly increased in PN-treated samples compared with those of control samples, which indicated PN induced the accumulation of protein ubiquitination (Fig. 4a).

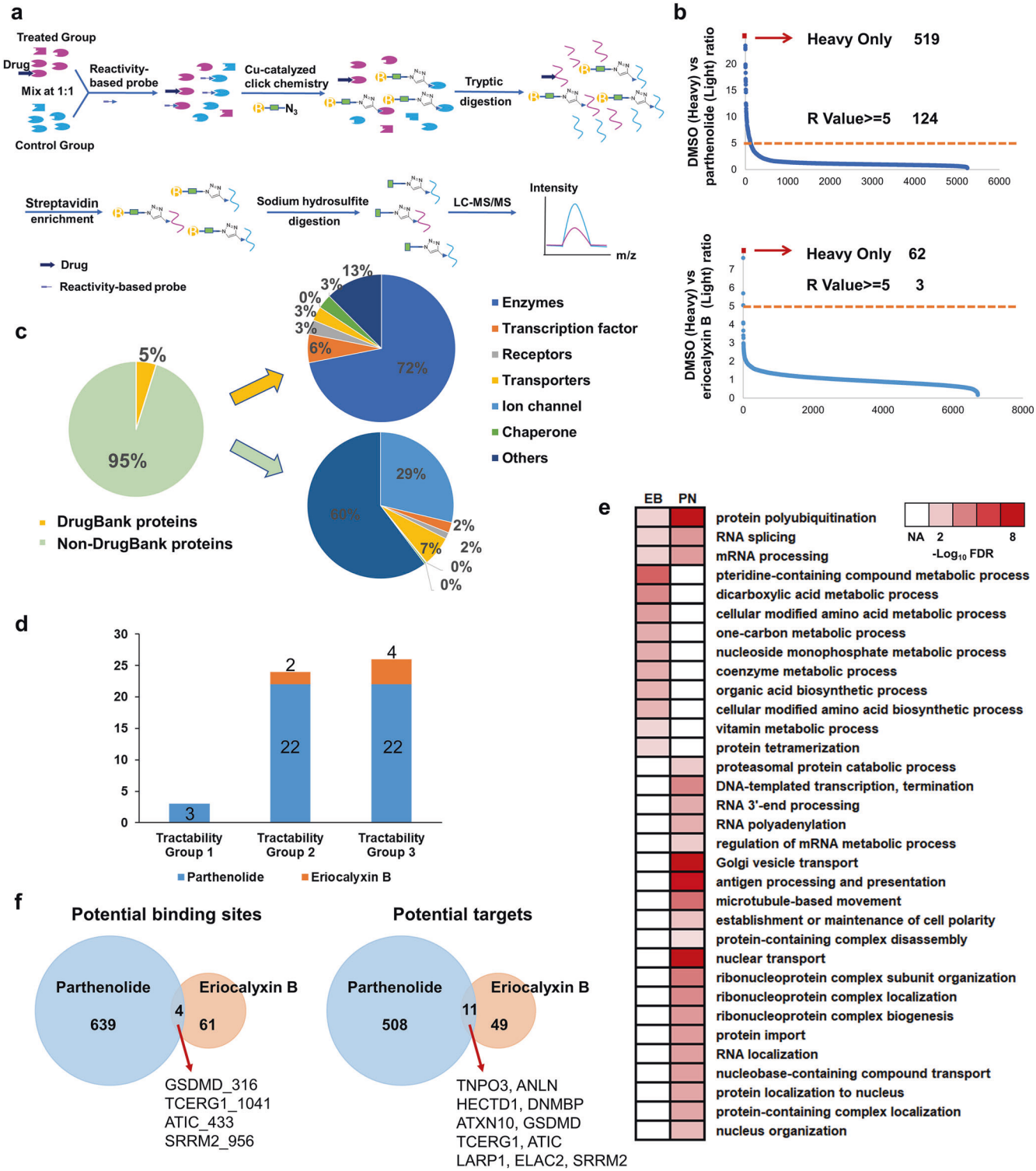

Fig. 3 ABPP to map EB and PN targets in MDA-MB-231 cells. a Competitive ABPP for quantitative mapping of potential covalent binding sites of targets. Treatment of cells with DMSO or EB/PN in situ, proteome labeling with an IA probe, Cu-catalyzed based click chemistry to incorporate biotin group, trypsin digestion, enrichment of probe-modified peptides with streptavidin, followed by sodium dithionite cleavage for LC-MS/MS analysis. **b** Distribution of competitive ABPP ratios (R values). Probe-modified peptides only occurred in heavy samples with good reproducibility, for which R values were assigned to maximum value. R value greater than 5 was shown by dashed lines to mark potential binding sites that exhibited high sensitivity to EB/PN. **(c)** Percentage of potential targets of EB and PN found in DrugBank proteins or Non-DrugBank proteins, and functional classification. **d** Overlap of potential targets with tractability group1/2/3 reported by other researchers. **e** Protein-protein interaction networks of the potential targets of EB and PN were analyzed respectively. The top 4 clusters of highly interconnected networks were performed GO Biological Process enrichment analysis. **f** The Venn diagram of shared binding sites and potential targets between EB and PN.

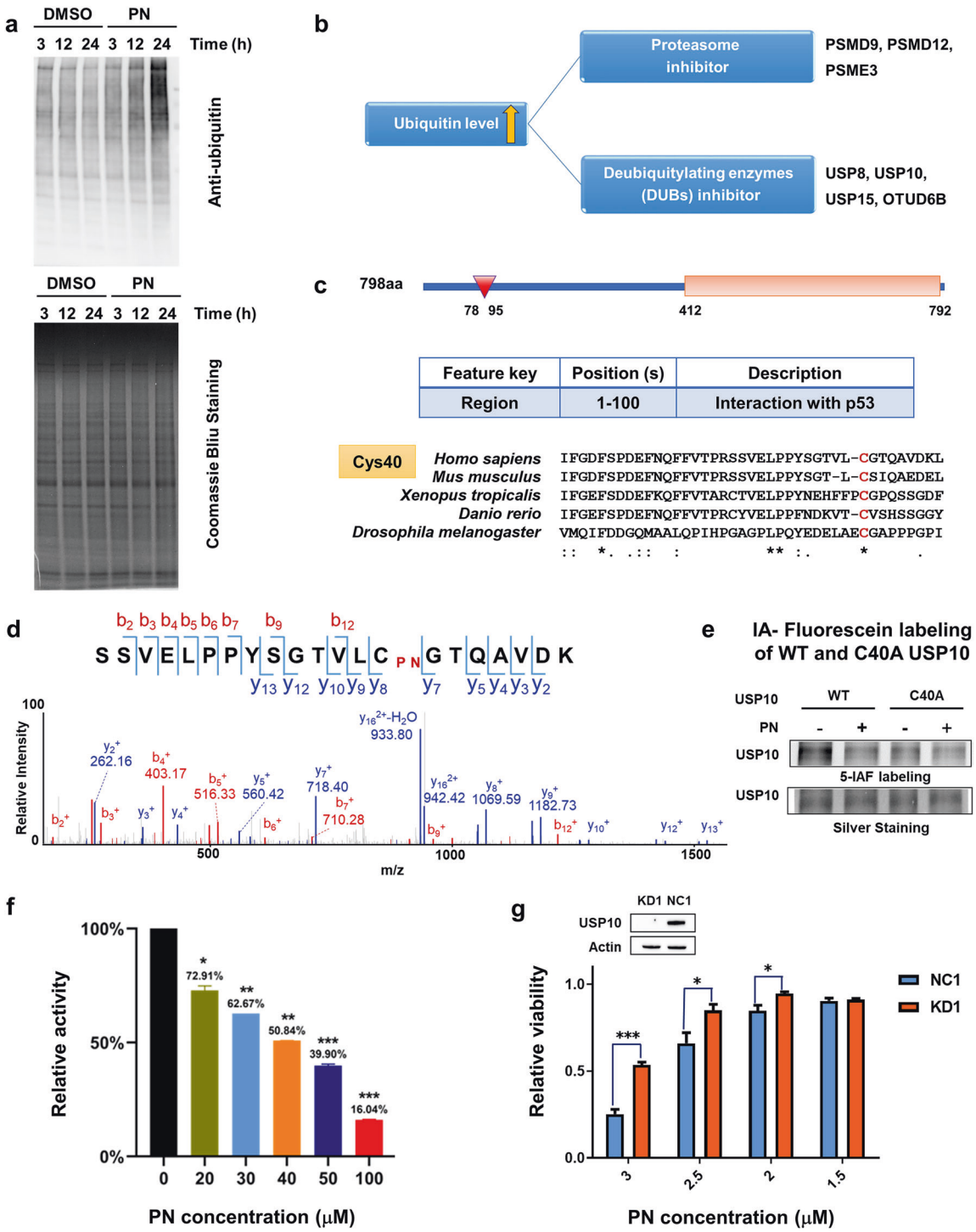

Fig. 4 **Biochemical validation of USP10 as a target of PN. a** Western blotting analyses of the whole cell lysate using anti-ubiquitin (pan) antibody were performed in control and PN-treated samples. Coomassie blue staining was used as the loading control. **b** The hypothesis that PN increased ubiquitin signals. **c** The critical regions for USP10 and sequence alignment of the potential binding site of Cys40 on USP10 among different species. **d** PN covalently bound to Cys40 on USP10. Purified USP10 (100 nM) was incubated with PN (10 μM) at room temperature for 30 min prior to LC-MS/MS analysis. **e** IA-Fluorescein labeling of WT and C40A USP10. Labeled proteins were scanned with Typhoon FLA 9500 scanner and silver staining was used as the loading control. **f** DUB activity assay kit was applied to measure USP10 activity. **(g)** USP10-knockdown MDA-MB-231 cells were constructed by lentiviral particles containing USP10 shRNA. USP10 expressions were validated by Western blotting of USP10-knockdown (KD) cells compared to negative control (NC) cells. Actin expressions were shown as loading control. The shown gel was from three biological replicates. Then, PN effects were assessed on USP10-knockdown cells and negative control cells. The shown data were a representative one from biological replicates. Data was shown as mean ± SEM. Statistical significance was calculated with unpaired two-tailed Student's *t*-tests. One asterisk indicates $P < 0.05$, two asterisks indicate $P < 0.01$ and three asterisks indicate $P < 0.001$.

Thus, we hypothesized that PN might be an inhibitor for proteasome or deubiquitinating enzymes. To this end, we focus on three proteasome regulatory subunits (PSMD9, PSMD12, and PSME3) and four deubiquitinating enzymes (USP8, USP10, USP15, and OTUD6B) in the list of PN potential targets (Fig. 4b). USP10 was involved in diverse cellular processes, including ubiquitin recycling, recycling of cellular proteins, stress granule formation, and DNA damage response [70]. More importantly, USP10 has crucial functions in tumor initiation and progression [71, 72]. Data from Cancer Dependence Map showed USP10 was essential in various cancer cell lines including MDA-MB-231 [73] (Supplementary Fig. S6b). Previous studies uncovered that the N-terminal region (1–100 amino acid) was critical for the interaction between USP10 and its substrate p53 [74]. Our results showed a potential covalently modified site at Cys40 on USP10, which is located exactly in this region and highly conserved among species (Fig. 4c).

To further validate PN covalently modified sites on USP10, we incubated purified USP10 with PN and then subjected to mass spectrometry analysis. We identified a number of peptides with a mass shift of 248.14 Da, which matched the molecular weight of the PN (Fig. 4d). This experiment demonstrated that PN covalently modified USP10 through Cys40, which is consistent with our ABPP results. In addition, we validated the interaction between PN and USP10 Cys40 through gel-based ABPP. Compared with wildtype protein, C40A mutant impacted 5-IAF labeling on USP10 (Fig. 4e). This experiment further confirmed that Cys40 in USP10 was a primary binding site for PN. Next, DUB activity assay kit was applied to assess whether PN could affect USP10 activity. The in vitro results showed PN exerted inhibitory effects on USP10 function in a concentration-dependent manner (Fig. 4f). Further, to determine whether the observed PN-mediated proliferative impairment was dependent on USP10, we evaluated PN effects on USP10-knockdown (KD) MDA-MB-231 cells. The results showed USP10 knockdown conferred significant resistance to PN-mediated cell growth inhibition compared with negative control (NC) cells (Fig. 4g). In addition, we compared ubiquitination differences between USP10KD/NC cells under PN treatment. Compared to USP10KD, NC cells exhibited stronger ubiquitination change with PN treatment (Supplementary Fig. S7). Collectively, we demonstrated PN inhibited the proliferation of MDA-MB-231 cells by, at least partially, covalently binding to USP10.

DISCUSSION

In this study, TMT-based quantitative proteomics analysis was performed to system-wide identify significantly differentially expressed proteins and the regulated pathways. Pathway enrichment analysis revealed that all these five natural products impacted the ubiquitin-mediated proteolysis pathways. Due to the higher activity on proliferation inhibition of EB and PN, we developed an ABPP platform to identify their preferentially modified targets as well as the exact covalent binding sites. Both quantitative proteomics and ABPP experiment implied that PN was associated with protein ubiquitination events, which was further validated by Western blotting analysis. USP10, a potential target for PN, was selected for further validation. The in vitro results showed PN covalently modified USP10 and exerted inhibitory effects on USP10 function. USP10-knockdown MDA-MB-231 cells conferred significant resistance to PN-mediated cell growth inhibition compared with negative control cells. These results demonstrated PN inhibited the proliferation of MDA-MB-231 cells by, at least partially, covalently binding to USP10. It is noteworthy that PN contains a α,β–unsaturated carbonyl group and an epoxide, both of which are capable of cysteine modification [16]. Further study on structure-activity relationship is warranted to elucidate the pharmacophore of this compound.

The protein expression changes of downstream substrates of USP10 in PN-treated samples showed the expression levels of RAF1, RPS2 and SKP2 were significant downregulated (P value < 0.05 and fold change <0.83). RAF1, is a key link between RAS activation and downstream MEK-ERK signaling, and involved in diverse cellular processes such as proliferation, differentiation, and apoptosis [75, 76]. RPS2 is overexpressed in malignant prostate cancer samples and might become a potential therapeutic target [77]. SKP2 is a substrate recognition component of a SCF (SKP1-CUL1-F-box protein) E3 ubiquitin-protein ligase complex, promoting breast cancer by degradation of programmed cell death protein 4 (PDCD4) [78]. A previous study demonstrated that SKP2 suppressed p53 protein level and inhibited PIG3-induced apoptosis [79]. Thus, we hypothesized that PN might inhibit USP10 to down-regulate the expression of SKP2 and subsequently increase the level of p53 for its anti-proliferation activity. Collectively, the substrate information expanded the basis for better understanding of the molecular mechanisms of PN.

Other targets could also contribute to anti-proliferation effect of PN in MDA-MB-231 cell line. Some well-studied PN targets like p65 and DNMT1 were also identified in our ABPP result. P65, a key transcriptional factor in NF-κB signaling pathway, was reported to be inhibited by PN at 5 μM [80]. And DNMT1, a key regulator of DNA methylation, was reported to be inhibited by PN at 3.5 μM [81]. They might participate in inhibitory effect on cell proliferation of PN at low concentration. Quantitative proteomics suggested that EB and PN may share similar molecular mechanisms in part by regulating protein ubiquitination, while the results of ABPP showed EB and PN may interact with different targets. In this study, we have demonstrated USP10 was one of PN targets. To obtain insight of possible mode of action for EB, we further investigated its potential targets. We analyzed protein-protein interaction networks of the EB potential targets and explored their underlying biological processes. Notably, the top enriched cluster was associated with protein polyubiquitination process, containing HECTD1, UBE2S and RNF213 (Supplementary Fig. S6c). E3 ubiquitin-protein ligases (HECTD1 and RNF213), as well as ubiquitin-conjugating enzyme E2S (UBE2S) are important for the development and progression of several types of cancer [78, 82–84]. Moreover, both HECTD1 and RNF213 were reported to mediate ubiquitination of IκBα, indicating they could participate in NF-κB signaling regulation of EB [85, 86]. These clues about EB potential targets might contribute to understanding the molecular mechanisms of EB-impaired breast cancer cell proliferation, which still need to be further validated using additional independent experiments.

In conclusion, this study uncovered the potential targets and molecular mechanisms of covalent inhibitors from natural sources, and provided a rich resource for drug discovery and development for triple-negative breast cancer.

DATA AVAILABILITY

All mass spectrometry raw data have been deposited in the iProX Consortium under the Subproject ID: IPX0003210000 and PXD number: PXD036046.

ACKNOWLEDGEMENTS

This work was supported by the National Key R&D Program of China (2020YFE0202200), the National Natural Science Foundation of China (32071432, 21907100, 22225702), the Program of Shanghai Academic Research Leader (22XD1420900), the Science and Technology Commission of Shanghai Municipality (19JC1416300), the Natural Science Foundation of China for Innovation Research Group (81821005), the Shanghai Sailing Program (21YF1456000), the open fund of state key laboratory of Pharmaceutical Biotechnology, Nanjing University, China (KF-202201), and the National Key R&D Program of China (2018YFC1705500).

AUTHOR CONTRIBUTIONS

MJT designed and supervised this study. WSZ performed the drug sensitivity experiments in cancer cell lines, TMT-based quantitative proteomics analysis, activity-based protein

profiling (ABPP) and bioinformatics analysis. ML and QY provided the compounds and participated in part of the designing and performing of the experiments. KFC and XLJ performed the biological validation experiments. YQH performed the bioinformatics analysis. WSZ wrote the manuscript, and KFC, BBH, HH, XYS, and MJT revised it.

ADDITIONAL INFORMATION

Supplementary information The online version contains supplementary material available at https://doi.org/10.1038/s41401-023-01072-z.

Competing interests: The authors declare no competing interests.

REFERENCES

1. Butler MS. Natural products to drugs: natural product-derived compounds in clinical trials. Nat Prod Rep. 2008;25:475–516.
2. Baker DD, Chu M, Oza U, Rajgarhia V. The value of natural products to future pharmaceutical discovery. Nat Prod Rep. 2007;24:1225–44.
3. Nomura DK, Maimone TJ. Target identification of bioactive covalently acting natural products. Curr Top Microbiol Immunol. 2019;420:351–74.
4. Kingston DGI. Modern natural products drug discovery and its relevance to biodiversity conservation. J Nat Prod. 2011;74:496–511.
5. Zhang T, Hatcher JM, Teng M, Gray NS, Kostic M. Recent advances in selective and irreversible covalent ligand development and validation. Cell Chem Biol. 2019;26:1486–500.
6. Lu Y, Chen B, Song JH, Zhen T, Wang BY, Li X, et al. Eriocalyxin B ameliorates experimental autoimmune encephalomyelitis by suppressing Th1 and Th17 cells. Proc Natl Acad Sci USA. 2013;110:2258–63.
7. Leung CH, Grill SP, Lam W, Gao W, Sun HD, Cheng YC. Eriocalyxin B inhibits nuclear factor-κB activation by interfering with the binding of both p65 and p50 to the response element in a noncompetitive manner. Mol Pharmacol. 2006;70:1946.
8. Qin GW, Xu RS. Recent advances on bioactive natural products from Chinese medicinal plants. Med Res Rev. 1998;18:375–82.
9. Freund RRA, Gobrecht P, Fischer D, Arndt HD. Advances in chemistry and bioactivity of parthenolide. Nat Prod Rep. 2020;37:541–65.
10. Ghantous A, Sinjab A, Herceg Z, Darwiche N. Parthenolide: from plant shoots to cancer roots. Drug Discov Today. 2013;18:894–905.
11. Liu M, Xiao CQ, Sun MW, Tan MJ, Hu LH, Yu Q. Xanthatin inhibits STAT3 and NF-κB signalling by covalently binding to JAK and IKK kinases. J Cell Mol Med. 2019; 23:4301–12.
12. Ju A, Cho YC, Cho S. Methanol extracts of Xanthium sibiricum roots inhibit inflammatory responses via the inhibition of nuclear factor-κB (NF-κB) and signal transducer and activator of transcription 3 (STAT3) in murine macrophages. J Ethnopharmacol. 2015;174:74–81.
13. Dai Y, Chen SR, Chai L, Zhao J, Wang Y, Wang Y. Overview of pharmacological activities of *Andrographis paniculata* and its major compound andrographolide. Crit Rev Food Sci Nutr. 2019;59:S17–29.
14. Li ZZ, Tan JP, Wang LL, Li QH. Andrographolide benefits rheumatoid arthritis via inhibiting MAPK pathways. Inflammation. 2017;40:1599–605.
15. Wen L, Xia N, Chen X, Li Y, Hong Y, Liu Y, et al. Activity of antibacterial, antiviral, anti-inflammatory in compounds andrographolide salt. Eur J Pharmacol. 2014;740:421–7.
16. Gersch M, Kreuzer J, Sieber SA. Electrophilic natural products and their biological targets. Nat Prod Rep. 2012;29:659–82.
17. Wang L, Zhao WL, Yan JS, Liu P, Sun HP, Zhou GB, et al. Eriocalyxin B induces apoptosis of t(8;21) leukemia cells through NF-κB and MAPK signaling pathways and triggers degradation of AML1-ETO oncoprotein in a caspase-3-dependent manner. Cell Death Differ. 2007;14:306–17.
18. Wang Y, Ma X, Yan S, Shen S, Zhu H, Gu Y, et al. 17-Hydroxy-jolkinolide B inhibits signal transducers and activators of transcription 3 signaling by covalently cross-linking Janus kinases and induces apoptosis of human cancer cells. Cancer Res. 2009;69:7302.
19. Wang Y, Shen S-Y, Liu L, Zhang X-D, Liu D-Y, Liu N, et al. Jolkinolide B inhibits proliferation or migration and promotes apoptosis of MCF-7 or BT-474 breast cancer cells by downregulating the PI3K-Akt pathway. J Ethnopharmacol. 2022;282:114581.
20. Sohma I, Fujiwara Y, Sugita Y, Yoshioka A, Shirakawa M, Moon JH, et al. Parthenolide, an NF-κB inhibitor, suppresses tumor growth and enhances response to chemotherapy in gastric cancer. Cancer Genom Proteom. 2011;8:39–47.
21. Mathema VB, Koh YS, Thakuri BC, Sillanpää M. Parthenolide, a sesquiterpene lactone, expresses multiple anti-cancer and anti-inflammatory activities. Inflammation. 2012;35:560–5.
22. Liu M, Xiao C, Sun M, Tan M, Hu L, Yu Q. Parthenolide inhibits STAT3 signaling by covalently targeting Janus kinases. Molecules. 2018;23:1478.
23. Berdan CA, Ho R, Lehtola HS, To M, Hu X, Huffman TR, et al. Parthenolide covalently targets and inhibits focal adhesion kinase in breast cancer cells. Cell Chem Biol. 2019;26:1027–35.e22.
24. Shi TL, Zhang L, Cheng QY, Yu JS, Liu J, Shen YJ, et al. Xanthatin induces apoptosis by activating endoplasmic reticulum stress in hepatoma cells. Eur J Pharmacol. 2019;843:1–11.
25. Li L, Liu P, Xie Y, Liu Y, Chen Z, Geng Y, et al. Xanthatin inhibits human colon cancer cells progression via mTOR signaling mediated energy metabolism alteration. Drug Dev Res. 2022;83:119–30.
26. Tohkayomatee R, Reabroi S, Tungmunnithum D, Parichatikanond W, Pinthong D. Andrographolide exhibits anticancer activity against breast cancer cells (MCF-7 and MDA-MB-231 cells) through suppressing cell proliferation and inducing cell apoptosis via inactivation of ER-α receptor and PI3K/AKT/mTOR signaling. Molecules. 2022;27:3544.
27. Chou YJ, Lin CC, Hsu YC, Syu JL, Tseng LM, Chiu JH, et al. Andrographolide suppresses the malignancy of triple-negative breast cancer by reducing THOC1-promoted cancer stem cell characteristics. Biochem Pharmacol. 2022;206:115327.
28. Cravatt BF, Simon GM, Yates JR 3rd. The biological impact of mass-spectrometry-based proteomics. Nature. 2007;450:991–1000.
29. Federspiel JD, Codreanu SG, Goyal S, Albertolle ME, Lowe E, Teague J, et al. Specificity of protein covalent modification by the electrophilic proteasome inhibitor Carfilzomib in human cells. Mol Cell Proteom. 2016;15:3233.
30. Patterson SD, Aebersold RH. Proteomics: the first decade and beyond. Nat Genet. 2003;33:311–23.
31. Domon B, Aebersold R. Mass spectrometry and protein analysis. Science. 2006;312:212–7.
32. Barglow KT, Cravatt BF. Activity-based protein profiling for the functional annotation of enzymes. Nat Methods. 2007;4:822–7.
33. Niphakis MJ, Cravatt BF. Enzyme inhibitor discovery by activity-based protein profiling. Annu Rev Biochem. 2014;83:341–77.
34. Wang C, Weerapana E, Blewett MM, Cravatt BF. A chemoproteomic platform to quantitatively map targets of lipid-derived electrophiles. Nat Methods. 2014;11:79–85.
35. Lanning BR, Whitby LR, Dix MM, Douhan J, Gilbert AM, Hett EC, et al. A road map to evaluate the proteome-wide selectivity of covalent kinase inhibitors. Nat Chem Biol. 2014;10:760–7.
36. Wang J, Zhang CJ, Chia WN, Loh CC, Li Z, Lee YM, et al. Haem-activated promiscuous targeting of artemisinin in *Plasmodium falciparum*. Nat Commun. 2015;6:10111.
37. Niessen S, Dix MM, Barbas S, Potter ZE, Lu S, Brodsky O, et al. Proteome-wide map of targets of T790M-EGFR-directed covalent inhibitors. Cell Chem Biol. 2017;24:1388–400.e7.
38. Deng X, Weerapana E, Ulanovskaya O, Sun F, Liang H, Ji Q, et al. Proteome-wide quantification and characterization of oxidation-sensitive cysteines in pathogenic bacteria. Cell Host Microbe. 2013;13:358–70.
39. Backus KM, Correia BE, Lum KM, Forli S, Horning BD, González-Páez GE, et al. Proteome-wide covalent ligand discovery in native biological systems. Nature. 2016;534:570–4.
40. Fonović M, Verhelst SH, Sorum MT, Bogyo M. Proteomics evaluation of chemically cleavable activity-based probes. Mol Cell Proteom. 2007;6:1761–70.
41. Tian C, Sun R, Liu K, Fu L, Liu X, Zhou W, et al. Multiplexed thiol reactivity profiling for target discovery of electrophilic natural products. Cell Chem Biol. 2017;24:1416–27.e5.
42. Savitski MM, Mathieson T, Zinn N, Sweetman G, Doce C, Becher I, et al. Measuring and managing ratio compression for accurate iTRAQ/TMT quantification. J Proteome Res. 2013;12:3586–98.
43. Ow SY, Salim M, Noirel J, Evans C, Rehman I, Wright PC. iTRAQ underestimation in simple and complex mixtures: "the good, the bad and the ugly". J Proteome Res. 2009;8:5347–55.
44. Ow SY, Salim M, Noirel J, Evans C, Wright PC. Minimising iTRAQ ratio compression through understanding LC-MS elution dependence and high-resolution HILIC fractionation. Proteomics. 2011;11:2341–6.
45. Verhelst SH, Fonović M, Bogyo M. A mild chemically cleavable linker system for functional proteomic applications. Angew Chem Int Ed Engl. 2007;46:1284–6.
46. Xu FW, Xiao CQ, Lv X, Lei M, Hu LH. Two new dimmeric xanthanolides isolated from *Xanthiurn mogolium* Kitag plant. Tetrahedron Lett. 2017;58:1312–5.
47. Che CT, Zhou TX, Ma QG, Qin GW, Williams ID, Wu HM, et al. Diterpenes and aromatic compounds from *Euphorbia fischeriana*. Phytochemistry. 1999;52:117–21.
48. Xu G, Wang J, Wu Z, Qian L, Dai L, Wan X, et al. SAHA regulates histone acetylation, butyrylation, and protein expression in neuroblastoma. J Proteome Res. 2014;13:4211–9.
49. Weerapana E, Wang C, Simon GM, Richter F, Khare S, Dillon MB, et al. Quantitative reactivity profiling predicts functional cysteines in proteomes. Nature. 2010;468:790–5.
50. Dayon L, Hainard A, Licker V, Turck N, Kuhn K, Hochstrasser DF, et al. Relative quantification of proteins in human cerebrospinal fluids by MS/MS using 6-plex isobaric tags. Anal Chem. 2008;80:2921–31.

51. Cox J, Mann M. MaxQuant enables high peptide identification rates, individualized p.p.b.-range mass accuracies and proteome-wide protein quantification. Nat Biotechnol. 2008;26:1367–72.
52. Chen Y, Kwon SW, Kim SC, Zhao Y. Integrated approach for manual evaluation of peptides identified by searching protein sequence databases with tandem mass spectra. J Proteome Res. 2005;4:998–1005.
53. Shannon P, Markiel A, Ozier O, Baliga NS, Wang JT, Ramage D, et al. Cytoscape: a software environment for integrated models of biomolecular interaction networks. Genome Res. 2003;13:2498–504.
54. Jensen LJ, Kuhn M, Stark M, Chaffron S, Creevey C, Muller J, et al. STRING 8-a global view on proteins and their functional interactions in 630 organisms. Nucleic Acids Res. 2009;37:D412–6.
55. Bader GD, Hogue CW. An automated method for finding molecular complexes in large protein interaction networks. BMC Bioinform. 2003;4:2.
56. Wang J, Vasaikar S, Shi Z, Greer M, Zhang B. WebGestalt 2017: a more comprehensive, powerful, flexible and interactive gene set enrichment analysis toolkit. Nucleic Acids Res. 2017;45:W130–w7.
57. Zhang Y, Wang ZH, Liu Y, Chen Y, Sun N, Gucek M, et al. PINK1 inhibits local protein synthesis to limit transmission of deleterious mitochondrial DNA mutations. Mol Cell. 2019;73:1127.e5.
58. Hou S, Qu D, Li Y, Zhu B, Liang D, Wei X, et al. XAB2 depletion induces intron retention in POLR2A to impair global transcription and promote cellular senescence. Nucleic Acids Res. 2019;47:8239–54.
59. Kapanidou M, Curtis NL, Bolanos-Garcia VM. Cdc20: at the crossroads between chromosome segregation and mitotic exit. Trends Biochem Sci. 2017; 42:193–205.
60. Wang L, Zhang J, Wan L, Zhou X, Wang Z, Wei W. Targeting Cdc20 as a novel cancer therapeutic strategy. Pharmacol Ther. 2015;151:141–51.
61. Li X, Kong L, Yang Q, Duan A, Ju X, Cai B, et al. Parthenolide inhibits ubiquitin-specific peptidase 7 (USP7), Wnt signaling, and colorectal cancer cell growth. J Biol Chem. 2020;295:3576–89.
62. Gopal YN, Chanchorn E, Van Dyke MW. Parthenolide promotes the ubiquitination of MDM2 and activates p53 cellular functions. Mol Cancer Ther. 2009;8:552–62.
63. Li Z, Liu K, Xu P, Yang J. Benchmarking cleavable biotin tags for peptide-centric chemoproteomics. J Proteome Res. 2022;21:1349–58.
64. Martin BR, Wang C, Adibekian A, Tully SE, Cravatt BF. Global profiling of dynamic protein palmitoylation. Nat Methods. 2011;9:84–9.
65. Behan FM, Iorio F, Picco G, Gonçalves E, Beaver CM, Migliardi G, et al. Prioritization of cancer therapeutic targets using CRISPR-Cas9 screens. Nature. 2019;568:511–6.
66. Menendez JA, Lupu R. Fatty acid synthase (FASN) as a therapeutic target in breast cancer. Expert Opin Ther Targets. 2017;21:1001–16.
67. Ye F, Huang J, Wang H, Luo C, Zhao K. Targeting epigenetic machinery: emerging novel allosteric inhibitors. Pharmacol Ther. 2019;204:107406.
68. Maennling AE, Tur MK, Niebert M, Klockenbring T, Zeppernick F, Gattenlöhner S, et al. Molecular targeting therapy against EGFR family in breast cancer: progress and future potentials. Cancers. 2019;11:1826.
69. Zhang S, Ju X, Yang Q, Zhu Y, Fan D, Su G, et al. USP47 maintains the stemness of colorectal cancer cells and is inhibited by parthenolide. Biochem Biophys Res Commun. 2021;562:21–8.
70. Bhattacharya U, Neizer-Ashun F, Mukherjee P, Bhattacharya R. When the chains do not break: the role of USP10 in physiology and pathology. Cell Death Dis. 2020;11:1033.
71. Takayama KI, Suzuki T, Fujimura T, Takahashi S, Inoue S. Association of USP10 with G3BP2 inhibits p53 signaling and contributes to poor outcome in prostate cancer. Mol Cancer Res. 2018;16:846–56.
72. Grunda JM, Nabors LB, Palmer CA, Chhieng DC, Steg A, Mikkelsen T, et al. Increased expression of thymidylate synthetase (TS), ubiquitin specific protease 10 (USP10) and survivin is associated with poor survival in glioblastoma multiforme (GBM). J Neurooncol. 2006;80:261–74.
73. Meyers RM, Bryan JG, McFarland JM, Weir BA, Sizemore AE, Xu H, et al. Computational correction of copy number effect improves specificity of CRISPR-Cas9 essentiality screens in cancer cells. Nat Genet. 2017;49:1779–84.
74. Yuan J, Luo K, Zhang L, Cheville JC, Lou Z. USP10 regulates p53 localization and stability by deubiquitinating p53. Cell. 2010;140:384–96.
75. Borovski T, Vellinga TT, Laoukili J, Santo EE, Fatrai S, van Schelven S, et al. Inhibition of RAF1 kinase activity restores apicobasal polarity and impairs tumour growth in human colorectal cancer. Gut. 2017;66:1106–15.
76. Chen J, Fujii K, Zhang L, Roberts T, Fu H. Raf-1 promotes cell survival by antagonizing apoptosis signal-regulating kinase 1 through a MEK-ERK independent mechanism. Proc Natl Acad Sci USA. 2001;98:7783–8.
77. Wang M, Hu Y, Stearns ME. RPS2: a novel therapeutic target in prostate cancer. J Exp Clin Cancer Res. 2009;28:6.
78. Wang L, Liang Y, Li P, Liang Q, Sun H, Xu D, et al. Oncogenic activities of UBE2S mediated by VHL/HIF-1α/STAT3 signal via the ubiquitin-proteasome system In PDAC. Onco Targets Ther. 2019;12:9767–81.
79. Zhang W, Cao L, Sun Z, Xu J, Tang L, Chen W, et al. Skp2 is over-expressed in breast cancer and promotes breast cancer cell proliferation. Cell Cycle. 2016;15:1344–51.
80. García-Piñeres AJ, Castro V, Mora G, Schmidt TJ, Strunck E, Pahl HL, et al. Cysteine 38 in p65/NF-kappaB plays a crucial role in DNA binding inhibition by sesquiterpene lactones. J Biol Chem. 2001;276:39713–20.
81. Liu Z, Liu S, Xie Z, Pavlovicz RE, Wu J, Chen P, et al. Modulation of DNA methylation by a sesquiterpene lactone parthenolide. J Pharmacol Exp Ther. 2009;329:505–14.
82. Duhamel S, Goyette MA, Thibault MP, Filion D, Gaboury L, Côté JF. The E3 ubiquitin ligase HectD1 suppresses EMT and metastasis by targeting the +TIP ACF7 for degradation. Cell Rep. 2018;22:1016–30.
83. Wang X, Ye M, Wu M, Fang H, Xiao B, Xie L, et al. RNF213 suppresses carcinogenesis in glioblastoma by affecting MAPK/JNK signaling pathway. Clin Transl Oncol. 2020;22:1506–16.
84. Banh RS, Iorio C, Marcotte R, Xu Y, Cojocari D, Rahman AA, et al. PTP1B controls non-mitochondrial oxygen consumption by regulating RNF213 to promote tumour survival during hypoxia. Nat Cell Biol. 2016;18:803–13.
85. Piccolis M, Bond LM, Kampmann M, Pulimeno P, Chitraju C, Jayson CB, et al. Probing the global cellular responses to lipotoxicity caused by saturated fatty acids. Mol Cell. 2019;74:32–44.e8.
86. Li Y, Huang B, Yang H, Kan S, Yao Y, Liu X, et al. Latexin deficiency in mice upregulates inflammation and aggravates colitis through HECTD1/Rps3/NF-κB pathway. Sci Rep. 2020;10:1–14.